# Large-scale in vivo CRISPR screens identify SAGA complex members as a key regulators of HSC lineage commitment and aging

**AUTHORS:**
Michael S. Haney[1,2], Archana Shankar[1,2,†], Ian Hsu[3, †], Masashi Miyauchi[4,5, †], Róbert Pálovics[1,2, †], Hwei Minn Khoo[3], Kyomi J. Igarashi[4,5], Joydeep Bhadury[4,5,6],Christy Munson[1,2], Paul K. Mack[4,5], Tze-Kai Tan[4,5], Tony Wyss-Coray[1,2,7,8, ‡ ,*], Hiromitsu Nakauchi[4,5,9, ‡ ,*], Adam C. Wilkinson[3,4, ‡ ,*]

**AFFILIATIONS:**
[1]Department of Neurology and Neurological Sciences, Stanford University School of Medicine; Stanford, CA, USA
[2]Wu Tsai Neurosciences Institute, Stanford University; Stanford, CA, USA
[3]MRC Weatherall Institute of Molecular Medicine, University of Oxford; Oxford, UK
[4]Institute for Stem Cell Biology and Regenerative Medicine, Stanford University School of Medicine; Stanford, CA, USA
[5]Department of Genetics, Stanford University School of Medicine, Stanford, CA, USA
[6]Department of Laboratory Medicine, Institute of Biomedicine, Sahlgrenska Academy, University of Gothenburg; Gothenburg, Sweden
[7]ChEM-H, Stanford University; Stanford, CA, USA
[8]Paul F. Glenn Center for the Biology of Aging, Stanford University School of Medicine; Stanford, CA, USA
[9]Division of Stem Cell Therapy, Distinguished Professor Unit, The Institute of Medical Science, The University of Tokyo; Tokyo, Japan
[†]These authors contributed equally to this work
[‡] Co-senior authors
[*]Co-corresponding authors: adam.wilkinson@imm.ox.ac.uk; nakauchi@stanford.edu; twc@stanford.edu

**ABSTRACT:**
The biological mechanisms that sustain the vast blood production required for healthy life remain incompletely understood. To address this knowledge gap, we developed an in vivo hematopoietic stem cell (HSC)-based large-scale CRISPR knockout screening platform to enable the genetic interrogation of hematopoiesis and broad aspects of immune cell function in vivo. Targeting ~7000 genes with this methodology, we discovered SAGA complex members *Tada2b* and *Taf5l* as key regulators of HSC lineage commitment. Loss of *Tada2b* or *Taf5l* inhibited hematopoiesis in vivo and was associated with upregulation of interferon response gene expression. SAGA complex member expression is significantly reduced in aged HSCs and upregulated with heterochronic parabiosis, suggesting a novel mechanism of age-associated hematopoietic decline and rejuvenation. Our study provides a rich functional genetics resource of hematopoiesis regulators accessible through a public interactive database (www.hematopoiesiscrisprscreens.com), a novel mechanism regulating age-related decline of hematopoiesis, and a new methodology with broad applications to systematically probe the development and functions of the lymphohematopoietic system.

**MAIN TEXT:**

Hematopoietic stem cells (HSCs) are a rare bone marrow (BM) cell type that have the potential to self-renew or undergo lineage commitment and differentiate into one of the many hematopoietic and immune cell types[1-5]. As such, HSCs support the hematopoietic and immune systems throughout life, which play various essential roles in human health from oxygen supply to wound healing to defense against pathogens. Approximately ~$10^{11}$ new blood cells are generated per day in humans. Hematopoietic system function generally declines with age and can result in leukopenia, anemia, and leukemia[6,7], as well as other pathologies (e.g., atherosclerosis, osteoporosis). It is also one of the major drivers of declining immune cell function in aged individuals, predisposing aged individuals to infection and cancers[8]. Understanding the mechanisms of healthy and pathogenic hematopoiesis is therefore a key question in the field of hematology, stem cell biology, and gerontology. In particular, the tight regulation of gene expression is critical for healthy hematopoiesis[9,10]. However, there is still much to be explored about this process.

While hematopoietic stem and progenitor cell (HSPC)-derived hematopoiesis is a well characterized system, the application of methods to identify genetic regulators of this process through high-throughput genetic screens has been hampered by the rarity of these cells. In vivo pooled CRISPR/Cas9 knockout (KO) screens offer an efficient method to investigate thousands of genetic regulators for a range of biological processes[11], and have already been applied to a number of cell lines[12-14]. However, the application of this system to primary HSCs is considerably more challenging because of the large numbers of cells required to perform these screens[15]. To date, in vivo HSC CRISPR screens have been limited to sgRNA libraries targeting ~30 genes[16]. The potential applications of large-scale in vivo HSC CRISPR screens are abundant; from identifying regulators of self-renewal and hematopoiesis to investigating mechanisms in the full range of biological functions of mature HSC-derived immune cells or searching for synthetic lethality gene interactions in pre-malignant HSCs.

**Results:**

***In vivo HSC CRISPR KO screens identify novel regulators of hematopoiesis***

To gain new insight into the genetics of hematopoiesis, we optimized a large-scale ex vivo HSC expansion culture method[17,18] to generate sufficient HSC numbers for CRISPR KO screens. Here we refer to the cells in these cultures as HSCs; we acknowledge that these cultures include hematopoietic progenitor cells but for simplicity we will refers to these as HSC cultures. We performed CRISPR KO screens in 3-week expanded primary mouse HSC cultures by targeting ~7,000 genes in the functional categories of transcription factors, kinases, phosphatases, drug targets, and genes associated with apoptosis and cancer. To target these ~7,000 genes, we used sgRNA libraries with a total of ~70,000 gene-targeting sgRNAs (10 sgRNAs/gene) and ~5,000 control sgRNAs (**Extended data Fig. 1a**). Pooled primary HSC KO cultures were maintained for an additional 2 weeks, with cells collected at days 7 and 14 for sgRNA sequencing to track sgRNA library representation. At both timepoints, sgRNA sequencing confirmed high library representation with essentially all sgRNAs contained within the libraries detected (**Extended data Fig. 1b**). By comparing the sgRNA library composition in the ex vivo HSC cultures on days 7 and 14, we identified 560 statistically significant genes (10% FDR) that modify HSC maintenance and expansion (**Extended data Fig. 1c**).

We next reconstituted the hematopoietic system in vivo with these pools of gene KO HSCs by transplantation into lethally irradiated recipients (**Fig. 1a**). We transplanted 17x$10^6$ day-14 CRISPR library cells into 17 lethally irradiated mice, which resulted in high-level multi-lineage

donor peripheral blood chimerism (**Fig. Extended Data Fig. 1d**). After 10-weeks, bone marrow and spleen from these mice were collected, pooled, and various hematopoietic cell types purified for sgRNA sequencing: c-Kit$^+$Sca1$^+$Lineage$^-$ HSPCs, Mac1/Gr1$^+$ myeloid cells, CD4/CD8$^+$ T cells, B220$^+$ B cells, and Ter119$^+$ erythroid cells. Within all mature in vivo immune cells populations analyzed, we could detect >50% of the library sgRNAs (**Extended Data Fig. 1e**), and essentially all targeted genes remained represented within our screen results (**Extended Data Fig. 1f**). This enabled four pairwise screen comparisons of various HSPC-derived blood cells for putative regulators of hematopoiesis revealing genetic regulators of the lineage trajectory from HSPCs to myeloid cells, T-cells, B-cells, and erythroid cells (**Fig. 1b-e**). Unsupervised hierarchical clustering of the top screen hits revealed clusters of genes that uniformly inhibit or promote hematopoiesis when knocked out as well as genes that promote the differentiation of specific lineages when knocked out (**Fig. 1f)**. Surprisingly, we found a previously undescribed role for several genes in the SAGA complex[19] (also known as the STAGA complex), a relatively uncharacterized regulatory hub involved in gene regulation, chromatin modification, DNA damage repair, and signaling. Knockout of several members of the SAGA complex (*Tada2b*, *Taf5l*, *Tada1,* and *Taf6l*) strongly inhibit differentiation of all hematopoietic lineages when knocked out and at a level similar to knockouts of well-characterized regulators of hematopoiesis (e.g., *Runx1*[20]). Additionally, this screen approach enabled multiple direct pairwise comparisons between mature cell types (e.g., myeloid versus lymphoid cells), which revealed genes that appear to modify the differentiation of various immune cell lineages (**Fig. 1g-j**). These screen results may serve as a resource for the wider community investigating the mechanisms of hematopoiesis. To support interrogation of this dataset, we have created an interactive webapp (www.hematopoiesiscrisprscreens.com).

***SAGA complex members regulate hematopoiesis***

Members of the SAGA complex emerged from these screens as novel, potent regulators of hematopoiesis (**Fig. 2a,b**). We focused on validating two of these genes, *Tada2b* and *Taf5l*. *Tada2b* encodes a transcriptional adaptor protein that is thought to be a subunit of the histone acetyltransferase module of SAGA, while *Taf5l* encodes a TATA-box binding protein associated factor that forms part of the core module of SAGA[21]. Unlike the enzymatic subunits of SAGA (Kat2a, Usp22), which are found in multiple complexes, these structural subunits are thought to be specific to the SAGA complex. *Taf5l* is broadly expressed within normal hematopoiesis, while *Tada2b* expression is low in HSCs and multipotent progenitors (MPPs) but upregulated during lineage commitment (**Extended Data Fig. 2a**). We performed targeted *Tada2b* and *Taf5l* knockout via electroporation of pre-complexed ribonucleoprotein Cas9/sgRNA into wild-type HSC cultures and evaluated gene INDEL (KO) frequencies within the culture over time. We confirmed that for both genes, the KO alleles became dominant over time. These results confirmed that our screening method was capable of identifying functional regulators of HSC activity (**Fig. 2c,d)**. Consistent with these knockouts displaying a block in differentiation, we observed an increase in the frequency of CD201$^+$CD150$^+$KSL population (recently shown to mark HSCs ex vivo[22,23]) within the *Tada2b* and *Taf5l* KO cultures (**Fig. 2e,f)**.

To validate our in vivo screen findings, we next transplanted CD45.1$^+$ HSCs following *Tada2b* or *Taf5l* KO into CD45.2$^+$ recipients alongside 1 million CD45.1$^+$CD45.2$^+$ whole bone marrow cells (**Fig. 2g**). After 16-weeks, peripheral blood and bone marrow was analyzed. Similar high-level donor CD45.1$^+$ chimerism was seen in all conditions within the bone marrow c-Kit$^+$Sca1$^+$Lineage$^-$ (KSL) HSPC population**,** but consistent with the in vivo screen results, donor peripheral blood chimerism was significantly lower from the *Tada2b* and *Taf5l* KO HSCs than the controls, with

*Tada2b* KO displaying a stronger phenotype (**Fig. 2h, Extended Data fig. 2b**). Similar decreases were observed when KO (INDEL) frequencies were measured in the PB and bone marrow KSL (**Extended Data fig. 2d**). Additionally, further resolution of bone marrow populations confirmed that a similar drop in *Tada2b* and *Taf5l* KO donor chimerism was also present in the $Lin^+$ bone marrow (**Fig. 2i**). Strikingly, increased frequencies of KSL HSPCs within the bone marrow were observed in the *Tada2b* and *Taf5l* KO recipients (**Fig. 2j**), suggesting that the inhibited hematopoietic differentiation in the KO HSCs led to an expansion of the primitive HSPC pool.

Consistent with the inhibition of hematopoiesis in the KO cohorts, complete blood cell (CBC) counts also identified significant reductions in white blood cell (WBC) counts in the *Tada2b* and *Taf5l* KO recipients (**Fig. 2k**). Red blood cell (RBC) counts were also reduced in the *Tada2b* KO (**Fig. 2l**), but no change in platelet counts was observed (**Extended Data Fig. 2f**). However, no gross abnormalities in bone marrow structure were observed (**Extended Data fig. 2c**). Spleen morphology was also similar between control and KO cohorts, although spleen weight was slightly increased in the KO recipients (**Extended Data fig. 2e**). Together, these results confirmed *Tada2b* and *Taf5l* as novel functional HSC regulators that are required for normal hematopoiesis.

***Loss of Tada2b or Taf5l causes interferon response gene expression***

Given these striking functional phenotypes from the genetic ablation of *Tada2b* and *Taf5l*, we were interested to better understand the consequences of these gene knockouts at the molecular levels. We therefore performed single cell RNA-sequencing (scRNAseq) of control, *Tada2b* KO, and *Taf5l* KO HSC cultures at 14-days post-RNP electroporation. Consistent with the known heterogeneity of our HSC cultures, initial clustering analysis identified four major cell types: a population of cells with an HSC and multipotent progenitor-like gene signature (HSC/MPP), a population of cells with a common myeloid progenitor/granulocyte progenitor-like gene signature (CMP/GMP), a population of cells with a general myeloid progenitor cell-like gene signature (myeloid progenitor), and a population of cells with a megakaryocyte progenitor-like gene signature (MkP) (**Fig. 3a, Extended Data Fig. 3a,b**). Consistent with our in vivo KO validations, we observed reductions in the frequency of the more mature CMP/GMP and myeloid progenitor clusters in the KO cells compared to control cells and an increase in the HSC/MPP cluster (**Fig. 3b**). Surprisingly, the MkP cluster was 2-3-fold larger in the KOs. When pseudotime values were calculated for each cell with the HSC/MPP cluster set as the lowest pseudotime value, clusters more abundant in the control cells compared to the KO cells (such as CMP/GMP and myeloid progenitor clusters) had higher pseudotime values, suggesting a more differentiated state in the control cell populations compared to the KO cell populations (**Fig. 3c**).

To further investigate the molecular consequences within HSCs, we subclustered specifically on the HSC/MPP population. By combining this re-clustering with cell cycle analysis, we could identify sub-clusters resembling G1-phase HSCs, S-phase HSCs, G2-phase HSCs, as well as populations resembling MPPs, LMPPs, MkPs, MEPs, and CLPs (**Fig. 3d, Extended Data Fig. 3c,d**). While control and KO cells were found in all clusters, we observed differences in the proportions within these clusters (**Fig. 3e**). For example, we observed increases in G2-HSCs within our *Tada2b* KO and *Taf5l* KO cultures (**Fig. 3f,g**). To avoid cell cycle-associated transcriptional changes, we focused on gene expression differences within the G1-HSC cluster. We observed major differences in the transcriptional programs expressed in the *Tada2b* and *Taf5l* KOs (**Figs. 3h**). Gene Ontology (GO) pathway analysis identified major changes in interferon (IFN) signaling (**Fig. 3i,j**). For example, interferon response genes *Ifi44*, *Ddx60*, and *Oasl2*, were significantly upregulated in the KO settings (**Fig. 3k**). Significant upregulation of IFN-related gene sets was

also observed in other progenitor clusters, suggesting that loss of *Tada2b* or *Taf5l* led to a derepression of IFN response genes.

The derepression of IFN signaling following *Tada2b* and *Taf5l* KO corresponded to our in vivo transplantation assay results; in vivo IFN treatment has been shown to inhibit hematopoiesis[24-26]. These results also corresponded with the immunophenotype of the *Tada2b* and *Taf5l* KO cell cultures, where we observed upregulation of Sca1 (Ly6e) expression, a known IFN response gene (**Fig. 3k**). Indeed, similar upregulation of Sca1 was seen when IFNa was added to wild-type HSC cultures (**Fig. 3m**). Low dose IFNa (0.1ng/ml) in wild-type HSC cultures appeared to partially phenocopy the *Tada2b* and *Taf5l* KO cultures, with increased frequencies of $CD201^{+}CD150^{+}$KSL cells observed (**Fig. 3l,n**). In line with previous reports[27-29] however, higher concentrations of IFNa caused HSC toxicities (data not shown).

Intrinsic IFN response gene expression within HSCs has been proposed as a mechanism to suppress viral transduction efficiency[30]. Consistent with this study, we observed higher expression of IFN response genes in the HSC cluster within our control scRNAseq dataset than the progenitor clusters (**Extended Data Figs. 4a,b**). Interestingly, expression of *Tada2b* inversely correlated with expression of IFN response genes such as *Ifi44* within early hematopoiesis (**Extended Data Figs. 2a and 4c**). Based on these observations and the data presented above, we suggest a model where low expression of *Tada2b* in the HSC/MPP compartment plays a physiological role in sustaining the basal IFN response gene expression pattern and *Tada2b* upregulation during differentiation contributes to their downregulation. Our results also suggest that upregulation of *Tada2b* expression is needed to facilitate lineage commitment from the immature HSC/MPP state. Consistent with this idea, lentiviral-mediated *Tada2b* overexpression reduced the $CD201^{+}CD150^{+}$KSL fraction within the HSC cultures (**Fig. 3o**).

***HSC KO screen hits overlap with age-related differentially-expressed genes***

Given the well-characterized dysfunction of hematopoiesis in aging[6,7], we sought to intersect our functional CRISPR KO screen dataset with genes differentially expressed with age in HSCs (from scRNAseq datasets[31]; **Extended Data Fig. 5**). Intersecting these datasets identified ~100 genes, out of ~300 screen hits that overlap with the 9,285 HSC aging differentially expressed genes (DEGs) (**Fig. 4a)**. Most of these overlaps were genes that inhibited differentiation when knocked out and downregulated in aged HSCs. This suggests that numerous DEGs in aged HSCs may have functional consequences on hematopoiesis. By performing gene-ontology enrichment analysis of these overlapping genes, we found SAGA complex genes as one of the top enriched categories, with multiple members of the SAGA complex differentially expressed with age (**Fig. 4b)**. Protein-protein interaction networks of these overlapping genes also revealed members of the Ragulator-Rag complex (LAMTOR genes) and transcriptional regulators including *Runx1* and Mediator complex subunits (**Fig. 4c**). Further interrogation of these genes and pathways may provide new mechanistic insights into the age-related functional decline of the hematopoietic system.

Recent single cell studies examining heterochronic parabiosis have concluded that aged HSCs are among the most dramatically altered transcriptionally following exposure to the young environment[31,32]. By overlapping our functional CRISPR KO screen hits with the genes differentially expressed in heterochronic parabiosis, we predicted that we may be able to infer some of the functional consequences of the reported genes expression changes in this rejuvenating condition. To this end, we intersected our CRISPR KO screen hits with (1) HSC DEGs in normal aging, (2) HSC DEGs in heterochronic parabiosis in the aged mice that change in the opposite direction to normal aging (rejuvenation), and (3) HSC DEGs in heterochronic parabiosis in the

young mouse that change in the same direction compared to normal aging (accelerated cellular aging) (**Fig. 4d**). This identified ~50 screen hits that overlapped with the rejuvenation DEG signature and another ~50 screen hits that overlapped with the accelerated cellular aging signature (**Fig. 4e,f**).

In the rejuvenation DEG overlap, most genes go down with age and are upregulated upon heterochronic parabiosis (with the exception of *Rrad*, the only overlapping gene that had the functional effect when knocked out of promoting hematopoiesis) (**Fig. 4e**). This again illustrates the functional concordance between the gene expression changes and the functional effects of the knockout. We also noted distinct clusters within the patterns of myeloid and lymphoid DEG and screen hit overlaps (**Fig. 4e,f**), suggesting distinct mechanisms of age-related dysfunction in myeloid vs. lymphoid differentiation potential, a well-characterized phenotype of the aging immune system[6,8]. Members of the SAGA complex again appeared in the overlaps of DEGs altered in the rejuvenation and accelerated cellular aging paradigms. Upon closer inspection of the SAGA complex members, *Taf5l* and *Taf6l* responded significantly to the aging environment as well as to heterochronic parabioses. Both were downregulated with age and in young mice with heterochronic parabiosis, and upregulated in aged mice with heterochronic parabiosis (**Fig. 4g**). Together with the results from our perturbation assays in **Figures 2-3**, this data suggests that some of the dysfunction of hematopoiesis with age and rejuvenation with heterochronic parabiosis may be mediated through the expression of these SAGA complex members. Elucidating the mechanisms of regulation and activity in HSCs may therefore yield novel therapeutic targets for restoring hematopoietic function and immunological resilience in aging.

**Discussion:**

In this study, we developed and applied an in vivo platform for CRISPR library screening in mouse hematopoiesis. We validated this approach with a ~75,000 element KO library. From this screen, we identified and validated SAGA complex members, *Tada2b* and *Taf5l*, as novel regulators of hematopoiesis, from which we propose a new mechanism regulating HSC lineage commitment and aging. Surprisingly, we also found that SAGA complex members are transcriptionally regulated by the aged environment. Given the functional studies of the SAGA complex members we describe here, we predict that the SAGA complex member gene expression changes seen in parabiosis may restore hematopoietic function in aged mice exposed to young systemic environments. Since this systemic intervention can induce SAGA complex member gene expression in aged HSCs, elucidating this mechanism may lead to novel therapeutic targets for the age-related decline of hematopoietic function. We hope these novel biological insights and large-scale functional datasets will contribute to efforts to decipher mechanisms of normal and aberrant hematopoiesis, as well as efforts to develop novel rejuvenation therapies. More broadly, we expect that the methods developed here for in vivo HSC CRISPR screens will enable genetic screens for many immune functions within a living organism. For example, this approach enables novel screens for genetic regulators of hematopoietic and immune system regulation. These extend beyond screens for developmental regulators of immune cell formation to screens for discovering genetic modifiers of immune cell function (e.g., phagocytosis, cytokine expression, infection resolution), age-related dysfunction in the immune system (e.g., immune cell senescence), immune cell interactions with various organs or cancers, or studying the development and function of tissue-resident macrophages (e.g., microglia).

**REFERENCES:**


1 Osawa, M., Hanada, K., Hamada, H. & Nakauchi, H. Long-term lymphohematopoietic reconstitution by a single CD34-low/negative hematopoietic stem cell. *Science* **273**, 242-245 (1996).

2 Wilkinson, A. C., Igarashi, K. J. & Nakauchi, H. Haematopoietic stem cell self-renewal in vivo and ex vivo. *Nat Rev Genet*, doi:10.1038/s41576-020-0241-0 (2020).

3 Eaves, C. J. Hematopoietic stem cells: concepts, definitions, and the new reality. *Blood* **125**, 2605-2613, doi:10.1182/blood-2014-12-570200 (2015).

4 Morrison, S. J. & Scadden, D. T. The bone marrow niche for haematopoietic stem cells. *Nature* **505**, 327-334, doi:10.1038/nature12984 (2014).

5 Laurenti, E. & Göttgens, B. From haematopoietic stem cells to complex differentiation landscapes. *Nature* **553**, 418-426, doi:10.1038/nature25022 (2018).

6 Gazit, R., Weissman, I. L. & Rossi, D. J. Hematopoietic stem cells and the aging hematopoietic system. *Semin Hematol* **45**, 218-224, doi:10.1053/j.seminhematol.2008.07.010 (2008).

7 de Haan, G. & Lazare, S. S. Aging of hematopoietic stem cells. *Blood* **131**, 479-487, doi:10.1182/blood-2017-06-746412 (2018).

8 Rossi, D. J., Jamieson, C. H. & Weissman, I. L. Stems cells and the pathways to aging and cancer. *Cell* **132**, 681-696, doi:10.1016/j.cell.2008.01.036 (2008).

9 Wilkinson, A. C. & Gottgens, B. Transcriptional regulation of haematopoietic stem cells. *Adv Exp Med Biol* **786**, 187-212, doi:10.1007/978-94-007-6621-1_11 (2013).

10 Orkin, S. H. & Zon, L. I. Hematopoiesis: An evolving paradigm for stem cell biology. *Cell* **132**, 631-644, doi:Doi 10.1016/J.Cell.2008.01.025 (2008).

11 Barrangou, R. & Doudna, J. A. Applications of CRISPR technologies in research and beyond. *Nat Biotechnol* **34**, 933-941, doi:10.1038/nbt.3659 (2016).

12 Tzelepis, K. *et al.* A CRISPR Dropout Screen Identifies Genetic Vulnerabilities and Therapeutic Targets in Acute Myeloid Leukemia. *Cell Rep* **17**, 1193-1205, doi:10.1016/j.celrep.2016.09.079 (2016).

13 Bell, C. C. *et al.* Targeting enhancer switching overcomes non-genetic drug resistance in acute myeloid leukaemia. *Nat Commun* **10**, 2723, doi:10.1038/s41467-019-10652-9 (2019).

14 Yamauchi, T. *et al.* Genome-wide CRISPR-Cas9 Screen Identifies Leukemia-Specific Dependence on a Pre-mRNA Metabolic Pathway Regulated by DCPS. *Cancer Cell* **33**, 386-400 e385, doi:10.1016/j.ccell.2018.01.012 (2018).

15 Doench, J. G. Am I ready for CRISPR? A user's guide to genetic screens. *Nat Rev Genet* **19**, 67-80, doi:10.1038/nrg.2017.97 (2018).

16 Rodriguez-Fraticelli, A. E. *et al.* Single-cell lineage tracing unveils a role for TCF15 in haematopoiesis. *Nature* **583**, 585-589, doi:10.1038/s41586-020-2503-6 (2020).

17 Wilkinson, A. C. *et al.* Long-term ex vivo haematopoietic-stem-cell expansion allows nonconditioned transplantation. *Nature* **571**, 117-121, doi:10.1038/s41586-019-1244-x (2019).

18 Wilkinson, A. C., Ishida, R., Nakauchi, H. & Yamazaki, S. Long-term ex vivo expansion of mouse hematopoietic stem cells. *Nat Protoc* **15**, 628-648, doi:10.1038/s41596-019-0263-2 (2020).

19 Soffers, J. H. M. & Workman, J. L. The SAGA chromatin-modifying complex: the sum of its parts is greater than the whole. *Genes Dev* **34**, 1287-1303, doi:10.1101/gad.341156.120 (2020).

20 de Bruijn, M. & Dzierzak, E. Runx transcription factors in the development and function of the definitive hematopoietic system. *Blood* **129**, 2061-2069, doi:10.1182/blood-2016-12-689109 (2017).

21 Herbst, D. A. *et al.* Structure of the human SAGA coactivator complex. *Nat Struct Mol Biol* **28**, 989-996, doi:10.1038/s41594-021-00682-7 (2021).

22 Che, J. L. C. *et al.* A highly efficient reporter system for identifying and characterizing in vitro expanded hematopoietic stem cells. *bioRxiv*, 2021.2006.2018.448972, doi:10.1101/2021.06.18.448972 (2021).

23 Becker, H. J. *et al.* A Single Cell Cloning Platform for Gene Edited Functional Murine Hematopoietic Stem Cells. *bioRxiv*, 2022.2003.2023.485423, doi:10.1101/2022.03.23.485423 (2022).

24 Soza, A. *et al.* Neutropenia during combination therapy of interferon alfa and ribavirin for chronic hepatitis C. *Hepatology* **36**, 1273-1279, doi:10.1053/jhep.2002.36502 (2002).

25 Schmid, M. *et al.* Suppression of haematopoiesis during therapy of chronic hepatitis C with different interferon alpha mono and combination therapy regimens. *Gut* **54**, 1014-1020, doi:10.1136/gut.2004.057893 (2005).

26 Peck-Radosavljevic, M. *et al.* Rapid suppression of hematopoiesis by standard or pegylated interferon-alpha. *Gastroenterology* **123**, 141-151, doi:10.1053/gast.2002.34175 (2002).

27 Pietras, E. M. *et al.* Re-entry into quiescence protects hematopoietic stem cells from the killing effect of chronic exposure to type I interferons. *J Exp Med* **211**, 245-262, doi:10.1084/jem.20131043 (2014).

28 Baldridge, M. T., King, K. Y., Boles, N. C., Weksberg, D. C. & Goodell, M. A. Quiescent haematopoietic stem cells are activated by IFN-gamma in response to chronic infection. *Nature* **465**, 793-797, doi:10.1038/nature09135 (2010).

29 Essers, M. A. *et al.* IFNalpha activates dormant haematopoietic stem cells in vivo. *Nature* **458**, 904-908, doi:10.1038/nature07815 (2009).

30 Wu, X. *et al.* Intrinsic Immunity Shapes Viral Resistance of Stem Cells. *Cell* **172**, 423-438 e425, doi:10.1016/j.cell.2017.11.018 (2018).

31 Palovics, R. *et al.* Molecular hallmarks of heterochronic parabiosis at single-cell resolution. *Nature* **603**, 309-314, doi:10.1038/s41586-022-04461-2 (2022).

32 Ma, S. *et al.* Heterochronic parabiosis induces stem cell revitalization and systemic rejuvenation across aged tissues. *Cell Stem Cell* **29**, 990-1005 e1010, doi:10.1016/j.stem.2022.04.017 (2022).

33 Ochi, K., Morita, M., Wilkinson, A. C., Iwama, A. & Yamazaki, S. Non-conditioned bone marrow chimeric mouse generation using culture-based enrichment of hematopoietic stem and progenitor cells. *Nat Commun* **12**, 3568, doi:10.1038/s41467-021-23763-z (2021).

34 Morgens, D. W. *et al.* Genome-scale measurement of off-target activity using Cas9 toxicity in high-throughput screens. *Nat Commun* **8**, 15178, doi:10.1038/ncomms15178 (2017).

35 Sun, J. *et al.* Structural basis for activation of SAGA histone acetyltransferase Gcn5 by partner subunit Ada2. *Proc Natl Acad Sci U S A* **115**, 10010-10015, doi:10.1073/pnas.1805343115 (2018).

36 Wilkinson, A. C. *et al.* Cas9-AAV6 gene correction of beta-globin in autologous HSCs improves sickle cell disease erythropoiesis in mice. *Nat Commun* **12**, 686, doi:10.1038/s41467-021-20909-x (2021).

37 Mann, H. B. & Whitney, D. R. On a Test of Whether one of Two Random Variables is Stochastically Larger than the Other. *The Annals of Mathematical Statistics* **18**, 50-60 (1947).
38 Benjamini, Y. & Hochberg, Y. Controlling the False Discovery Rate: A Practical and Powerful Approach to Multiple Testing. *Journal of the Royal Statistical Society. Series B (Methodological)* **57**, 289-300 (1995).
39 Szklarczyk, D. *et al.* STRING v11: protein-protein association networks with increased coverage, supporting functional discovery in genome-wide experimental datasets. *Nucleic Acids Res* **47**, D607-D613, doi:10.1093/nar/gky1131 (2019).
40 Kuleshov, M. V. *et al.* Enrichr: a comprehensive gene set enrichment analysis web server 2016 update. *Nucleic Acids Res* **44**, W90-97, doi:10.1093/nar/gkw377 (2016).
41 Seita, J. *et al.* Gene Expression Commons: an open platform for absolute gene expression profiling. *PLoS One* **7**, e40321, doi:10.1371/journal.pone.0040321 (2012).

**ACKNOWLEDGMENTS:**
We thank the Stanford Stem Cell Institute FACS Core and WIMM Flow Cytometry Core for flow cytometry access, the Stanford Animal Histology Service for histology, the CZ-Biohub for performing the next generation sequencing, and the WIMM Genome Engineering Core for plasmid cloning. We thank Amanda Ghassaei for assistance with the interactive webapp and figures. A.C.W. acknowledges supported from the NIH (K99HL150218), the Leukemia and Lymphoma Society (3385-19), the Edward P. Evans Foundation, and the Kay Kendall Leukaemia Fund. H.N. was supported by the NIH (R01DK116944; R01HL147124), the Ludwig Foundation, and the Japan Society of the Promotion of Science. J.B. was supported by international postdoc grant (2017-0034) from the Swedish Research Council and the Assar Gabrielsson Foundation, Sweden. M.S.H acknowledges support from the Buck Institute and NIA (T32AG000266). T.W.C. acknowledges support from the NIH (AG072255).

**AUTHORSHIP CONTRIBUTIONS:**
MH, AS, IH, MM, CM, HMK, KJI, RP, JB, PKM, TKT and ACW performed experiments and analyzed data. MH, HN, TWC, and ACW wrote the manuscript. All authors reviewed and edited the manuscript.

**COMPETING INTERESTS:**
H.N. is a co-founder and shareholder in ReproCELL, Megakaryon, and Century Therapeutics. However, none of these companies had input into the design, execution, interpretation, or publication of the work in this manuscript.

**DATA AVAILABILITY:**
Data supporting the findings of this work are available within the paper and its Supplementary Information files. The datasets and materials generated and analyzed during the current study are available from the corresponding author upon request. We have made CRISPR screening datasets publicly accessible via an interactive web app: www.hematopoiesiscrisprscreens.com.

## METHODS:

### Mice

All animal experiments were approved by the Administrative Panel on Laboratory Animal Care at Stanford University or performed in accordance with UK Home Office regulations. C57BL/6-Rosa26$^{CAG\text{-}Cas9}$ (B6J.129(Cg)-Gt(ROSA)26Sor$^{tm1.1(CAG\text{-}cas9*,\text{-}EGFP)Fezh/J}$; 026179) and C57BL/6-CD45.1 (PepboyJ; 002014) were purchased from The Jackson Laboratory. C57BL/6-CD45.2 mice purchased from The Jackson Laboratory (000664) or bred at the University of Oxford. C57BL/6-CD45.1/CD45.2 F1 mice were bred from C57BL/6-CD45.1 and C57BL/6-CD45.2 at Stanford University. All mice were 8-12 weeks at the experiment start point.

### Ex vivo HSC cultures

HSC cultures were initiated from c-Kit$^+$ bone marrow[33] from C57BL/6-Rosa26$^{CAG\text{-}Cas9}$ mice. Tibia, femur, pelvis, and vertebrae were collected and crushed to release bone marrow cells. Bone marrow was then stained with c-Kit-microbeads (Miltenyi) and c-Kit$^+$ cells enriched via MACS column (Miltenyi) according to the manufacturer's protocol. Enriched c-Kit$^+$ bone marrow cells were cultured in HSC expansion media with complete media changes every 2-3 days and split 1:2 after 2-weeks. HSC expansion media composition[17,18]: Ham's F12 media (Gibco) supplemented with 1X penicillin-streptamycin-glutamine (Gibco), 1X HEPES (Gibco), 1X insulin-transferrin-selenium-ethanolamide (Gibco), 1 mg/ml polyvinyl alcohol (Sigma), 100 ng/ml recombinant mouse thrombopoietin (Peprotech), and 10 ng/ml recombinant mouse stem cell factor (Peprotech).

### Ex vivo and in vivo CRISPR screen

After 3-week ex vivo expansion of c-Kit$^+$ bone marrow HSCs, ~50 million cells were transduced overnight with lentivirus generated from the (1) Gene Expression, (2) Apoptosis and Cancer, or (3) Drug Targets, Kinases, Phosphatases CRISPR knockout libraries[34] (a kind gift from the Bassik lab; Addgene 1000000121-1000000123) generated using helper plasmids pCMV-VSV-G-RSV-Rev and pMDLg/pRRE. To reduce multiple integrations per cell, we used a transduction efficiency of 20%. Two days later, transduced HSCs were selected for using puromycin for 72 hours. HSCs were maintained in culture for a total of 14 days post-transduction. At day 14, HSCs were transplanted into 17 lethally-irradiated (10Gy) C57BL/6-CD45.1 recipients (1 million HSCs per recipient). After 10-weeks, mouse whole bone marrow and spleen were harvested. From whole bone marrow, c-Kit$^+$Sca1$^+$Lineage$^-$ HSCs were isolated by FACS. The remaining bone marrow and spleen was pooled and CD45R$^+$ B cells, CD4/CD8$^+$ T cells, Mac1/Gr1$^+$ myeloid cells, and Ter119$^+$ erythroid cells were isolated via MACS columns.

### Screen analysis

Genomic DNA was extracted for all screen populations separately according to the protocol included with QIAGEN Blood Mini or Midi Kit. Using known universal sequences present in the lentivirally incorporated DNA, sgRNA sequences were amplified and prepared for sequencing by two sequential PCR reactions as previously described[34]. Products were sequenced using an Illumina Nextseq to monitor library composition (20–40 million reads per sample). Trimmed sequences were aligned to libraries using Bowtie, with zero mismatches tolerated and all alignments from multi-mapped reads included. Guide composition and comparisons across each cellular fraction were analyzed using CasTLE version 1.0[34]. Briefly, enrichment of individual sgRNAs was then calculated as a median-normalized log ratio of the fraction of counts. For each gene, a maximum likelihood estimator was used to identify the most likely effect size and associated log-likelihood ratio (confidence score) by comparing the distribution of gene-targeting

guides to a background of nontargeting and safe-targeting guides. P-values were then estimated by permuting gene-targeting guides, and hits were called using FDR thresholds calculated via the Benjamini-Hochberg procedure. Gene enrichment analysis was performed using the top 200 ranked hits promoting or inhibiting HSC state by confidence score using EnrichR. SAGA complex structure heatmap (**Fig. 2b**) made with PyMol by coloring structural subunits with effect scores and p-values from screen computed by CasTLE. The following PDB files were used for the SAGA complex structure: 6CWD[35] and 7KTR[21].

**Ex vivo validation assays**

To generate *Taf5l* or *Tada2b* KO HSCs, 2x10$^5$ HSCs derived from two-week C57BL/6 c-Kit$^+$ bone marrow (as described in the **Ex vivo HSC culture** section) were electroporated with 6ug recombinant HiFi Cas9 (IDT) pre-complexed with 3.2ug synthetic sgRNA (Synthego) using a Lonza 4D-Nucleofector using program EO100 in primary P3 solution and then returned to HSC expansion media[36]. Electroporation of Cas9 only or *Rosa26*-targeting RNP were used as controls. At indicated timepoints, cells were collected for KO frequencies or flow cytometry analysis. To determine KO frequencies, gDNA was isolated via QuikExtract for PCR and Sanger sequencing with KO frequencies determined using ICE software (Synthego). For flow cytometric analysis, cells were antibody stained (CD201-APC, CD150-PE/Cy7, cKit-BV421, Sca1-PE, Gr1-APC/eFluor780, Ter119-APC/eFluor780, CD4-APC/eFluor780, CD8-APC/eFluor780, CD45R-APC/eFluor780, CD127-APC/eFluor780) for 30 minutes at 4°C, washed and then analyzed using a LSRFortessa (BD) with propidium iodide (Biolegend) as a live/dead cell stain. Alternatively, lentivirus carrying sgRNAs (cloned into pMCB306; a kind gift from the Bassik lab), Tada2b-2A-GFP cDNA, or GFP cDNA were generated and transduced into Cas9-expressing (or wild-type) C57BL/6 HSCs, as described in the **Ex vivo and in vivo CRISPR screen** section. For interferon studies, two-week C57BL/6 c-Kit$^+$ bone marrow cells were cultured in media with recombinant mouse interferon alpha (Biolegend) as indicated with media changes every 2-3 days. Flow cytometric analysis was then performed following antibody staining (CD201-APC, CD150-PE/Cy7 cKit-BV421, Sca1-PE, Gr1-FITC, Ter119-FITC, CD4-FITC, CD8-FITC, CD45R-FITC, CD127-FITC) for 30 minutes at 4°C, washed and then analyzed using a LSRFortessa (BD) using propidium iodide (Biolegend) as a live/dead cell stain. All flow cytometric data analysis was performed using FlowJo and statistical analysis performed using Prism.

**HSC transplantation assays**

CD150$^+$CD34$^-$Kit$^+$Sca1$^+$Lineage$^-$ HSCs were isolated using a FACSAriaII (BD) from C57BL/6-CD45.1 bone marrow and electroporated with either Cas9/sgRNA targeting *Tada2b*, *Taf5l*, or *Rosa26* (same protocol as **Ex vivo validation assays** section) and then expanded for 7-days before transplantation into five lethally-irradiated (10 Gy) C57BL/6-CD45.2 recipient mice (500 HSC equivalent per recipient) alongside 1 million whole bone marrow competitor cells isolated from C57BL/6-CD45.1/CD45.2 F1 mice. Peripheral blood samples were analyzed using a Horiba Micros ESV 60 complete blood counter or by flow cytometry. For flow cytometry, peripheral blood leukocytes were stained with antibodies (CD45.1-PE/Cy7, CD45.2-BV421, Mac1-PE, Gr1-PE, CD45R-APC/Cy7, CD4-APC, CD8-APC) following red blood cell lysis. Samples were then run on an FACSAriaII or LSRFortessa using propidium iodide as a live/dead cell stain, with CD45.1$^+$ cells sorted for KO analysis. Data analysis was performed using FlowJo. At the endpoint, bone marrow and spleen were collected and fixed (4% paraformaldehyde for 48 hours) for hematoxylin and eosin staining (performed by the Stanford Animal Histology Service). Bone marrow chimerism was also analyzed by sequential antibody staining with a lineage cocktail (Gr1-

biotin, Ter119-biotin, CD4-biotin, CD8-biotin, CD45R-biotin, CD127-biotin) followed by Streptavidin-APC/eFluor780, CD34-FITC, c-Kit-APC, Sca1-PE, CD45.1-PE/Cy7, CD45.2-BV421). Samples were then run on an FACSAriaII or LSRFortessa using propidium iodide as a live/dead cell stain, with CD45.1$^+$c-Kit$^+$Lineage$^-$ cells sorted for KO analysis. All flow cytometric data analysis was performed using FlowJo and statistical analysis performed using Prism.

**Single-cell RNAseq analysis**

At day-14 post-electroporation, control, *Tada2b* KO, or *Taf5l* KO HSC cultures were collected for RNA-seq analysis using a Gene Expression kit v3 (10x Genomics) according to the manufacturer's protocol with libraries sequenced on a NovaSeq 6000 S4 (Illumina). Raw gene counts were obtained by aligning reads to the mouse genome using CellRanger software (v.4.0.0) (10x Genomics). For quality control, cells with unique feature counts over 2,500 or less than 200 were removed as well as cells that have >5% mitochondrial counts. Ambient cell free mRNA contamination was removed using SoupX for each individual sample. Multiplets were filtered out using DoubletFinder. The core statistical parameters of DoubletFinder (nExp and pK) used to build artificial doublets for true doublet classification were determined automatically using recommended settings. The SCTransform-based integration workflow of Seurat was used to align data, using default settings. In brief, the integration workflow searches for common gene modules (anchors) in cells with similar transcriptomes. Individual samples after undergoing quality control are integrated in a step-wise fashion, using cellular sequencing depth as a covariate to mitigate technical artefacts. After combining the samples into a single dataset or Seurat object, genes were projected into principal component space using the principal component analysis (RunPCA). The first 100 dimensions were used as inputs into the FindNeighbours, FindClusters and RunUMAP functions of Seurat. In brief, a shared-nearest-neighbor graph was constructed based on the Euclidean distance metric in principal component space, and cells were clustered using the Louvain method. RunUMAP functions with default settings was used to calculate 2D UMAP coordinates and search for distinct cell populations. Distinct cell populations were annotated based on conical marker genes. Monocle3 (v.0.2.1.) was used to generate the pseudotime trajectory analysis of HSCs. Cells were re-clustered as described in and used as input into Monocle to infer cluster and lineage relationships within a given cell type. Specifically, UMAP embeddings and cell subclusters generated from Seurat were converted to a cell_data_set object using SeuratWrappers (v.0.2.0) and then used as input to perform trajectory graph learning and pseudotime measurement through reversed graph embedding with Monocle. Cell cycle analysis was performed in Seurat using a list of cell cycle markers from Tirosh et al[34]. Differential gene expression was performed in Seurat using MAST package under default conditions.

**Aging and parabiosis single-cell RNAseq analysis**

We performed differential gene expression based on the data and methods of a recent single-cell study on aging (AGE) and parabiosis[31] (accelerated aging: ACC and rejuvenation: REJ). We investigated 3 comparisons (AGE: Y-A, ACC: IY-HY, REJ: IA-HA) within the marrow HSCs and used the processed log-CPM data of the aforementioned study[31]. We calculated standard log2-fold changes and performed non-parametric unpaired Wilcoxon–Mann–Whitney test[37] for each gene. Two-sided p-values were corrected with Benjamini-Hochberg procedure[38] (FDR=0.05) per comparison. Finally, we identified genes differentially expressed with adjusted p-value<0.05. We discarded genes used for QC filtering (Rb* and Mt-*) from the DGE analysis since these may be biased by the QC process.

When intersecting the results with the screen data, first we considered genes that are significant in both datasets with adjusted p-value<0.05. Next, we identified genes that show similar changes with AGE and in the screen data (i.e., both upregulated or downregulated). Additionally, we selected the subset of those that either changed in the *same* direction with AGE and ACC or changed in the opposite direction with AGE and REJ.

For each differentially expressed gene set of interest, we queried the STRING database[39] for links with confidence values>0.7 (noted as "high confidence" in STRING) and queried Enrichr[40] for pathways with adj. p-value<0.05 of the Gene Ontology Cellular Components 2021 database.

# FIGURES AND LEGENDS:

## Figure 1

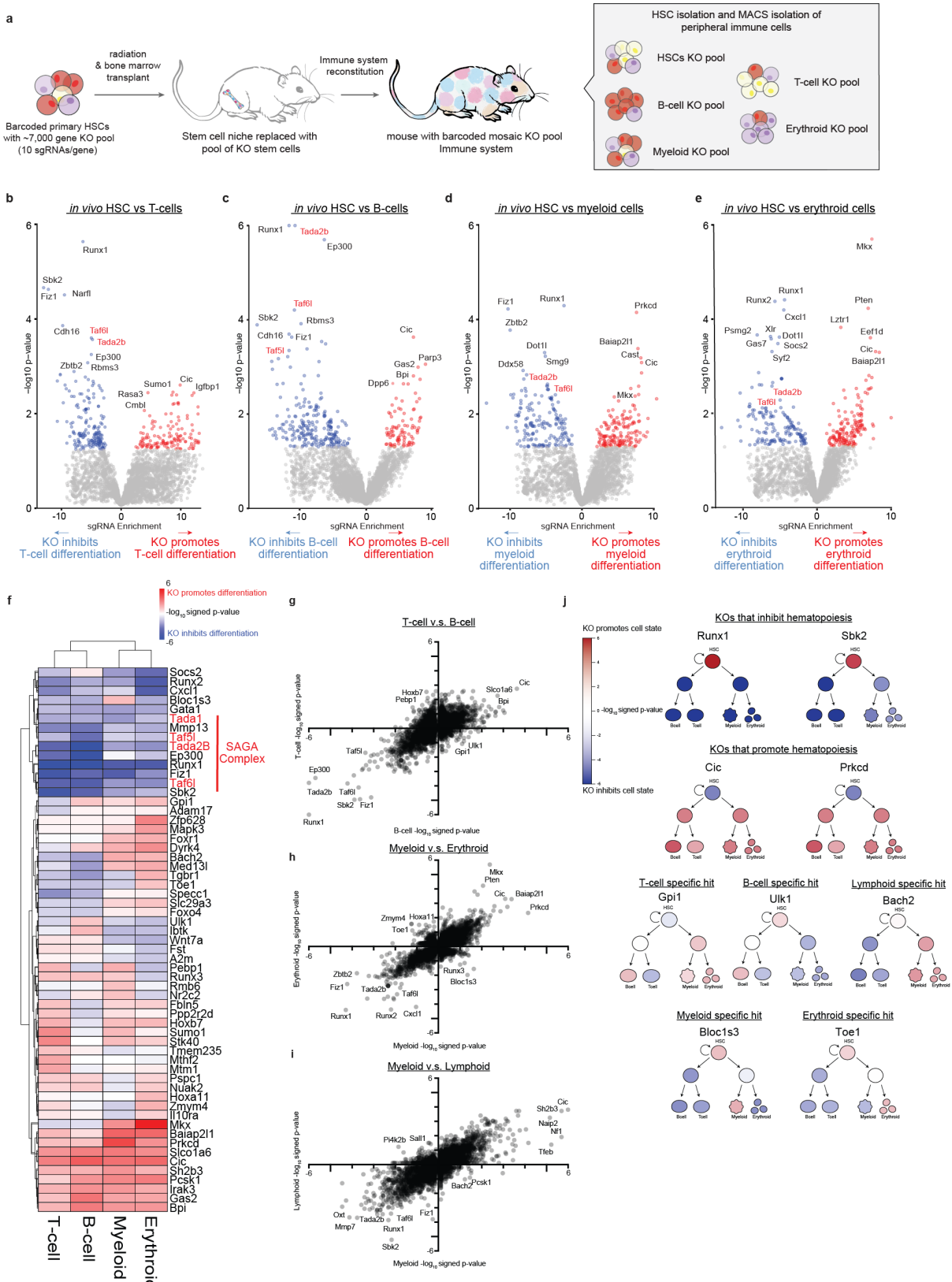

**Fig. 1: In vivo CRISPR KO screens in primary HSCs identifies novel regulators of hematopoiesis. a,** In vivo CRISPR KO screening schematic. **b-e,** Volcano plot showing in vivo HSC CRISPR screen results comparing HSPC KOs with KO mature T-cells (**b)**, mature B-cells (**c**), myeloid cells (**d**), and erythroid cells (**e**). All ~7,000 gene KOs displayed the effect of KO (negative if KO enriched in HSPCs, positive if KO enriched in differentiated cells) on the x axis and $\log_{10}$(p-value) on the y axis. Effect and p-values determined by casTLE and genes with a p-value < 0.05, colored red for positive effect scores or blue for negative effect scores. SAGA complex members labeled in red. **f,** Unsupervised hierarchical clustering of select CRISPR screen hits. SAGA complex members highlighted in red. **g-i,** Scatterplots comparing screen hits between T-cell and B-cell screen results (**g**), myeloid and erythroid screen results (**h**), and myeloid and lymphoid cells (**i**). **j,** Hematopoietic tree schematic overlayed with effect gene KO on differentiation potential of four mature cell lineages.

Figure 2

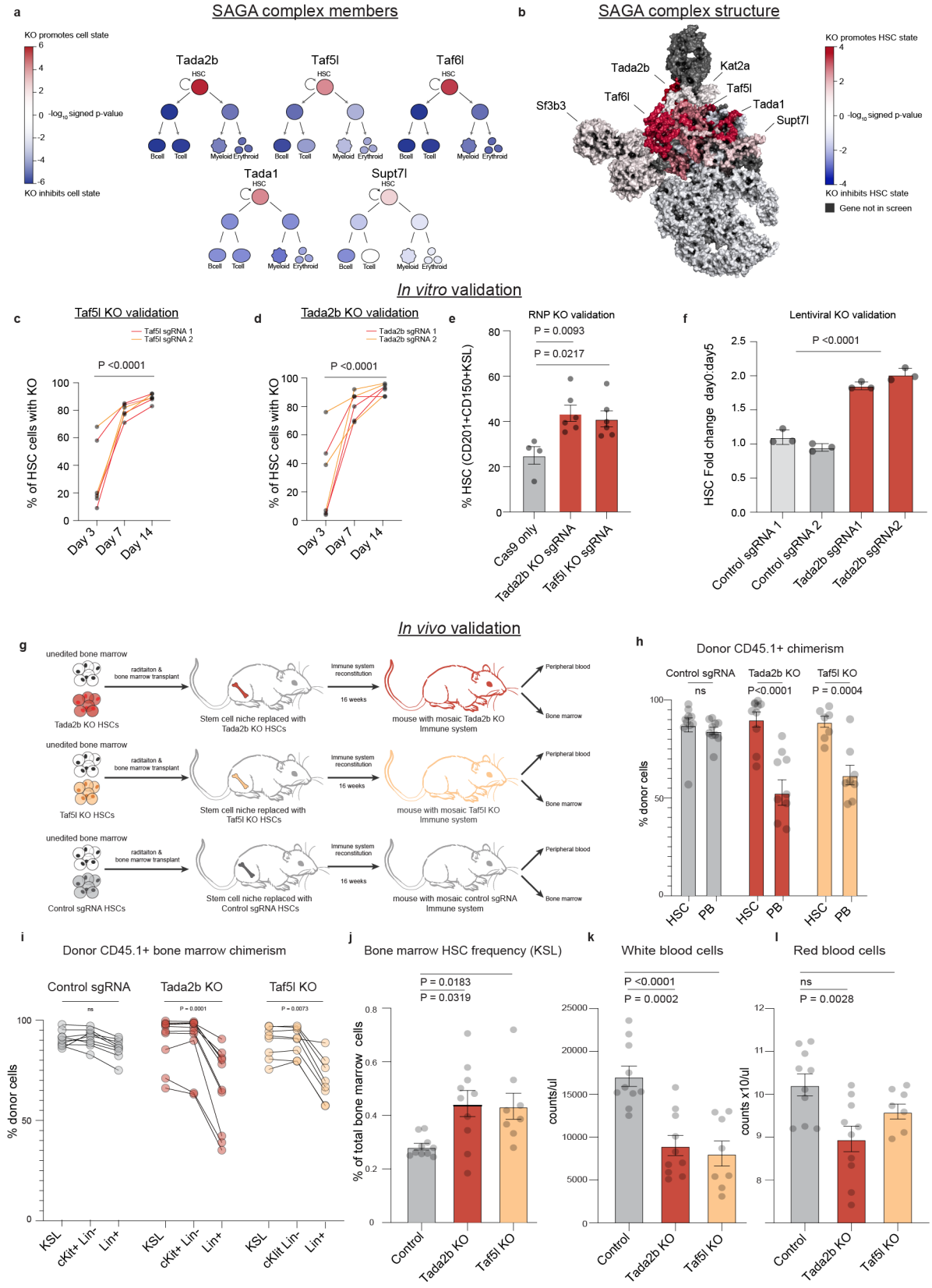

**Fig. 2: Loss of SAGA complex members *Tada2b* and *Taf5l* cause inhibition of hematopoiesis. a,** Hematopoietic tree schematic showing the effect of SAGA complex member KOs on hematopoiesis. **b,** Structure of SAGA complex[21,35] overlayed with heatmap with screen results displaying signed $Log_{10}$ (p-value) for KO effect on hematopoiesis. **c-d,** Allelic KO scores for *Taf5l* (**c**), *Tada2b* (**d**) following Cas9/sgRNA mutation of these genes at day 3, day 7, day 14. Three biological replicates for two sgRNAs are displayed. P-values determined by paired t-test. **e,** Percentage of phenotypic HSCs ($CD201^+CD150^+KSL$) in ex vivo cultures following RNP KO of SAGA complex members. Six biological replicates with two independent sgRNAs displayed. P-values determined by ANOVA. **f,** Fold change of phenotypic HSCs in ex vivo cultures following lentiviral KO of *Tada2b*. Three biological replicates per condition are displayed. P-values determined by paired t-test. **g,** Schematic for in vivo competitive transplantation assay validation experiments. $CD45.1^+$ *Tada2b* KO, *Taf5l* KO, and control HSCs were transplanted against 1 million $CD45.1^+CD45.2^+$ whole bone marrow competitor cells into lethally irradiated $CD45.2^+$ recipient mice, with donor chimerism analyzed after 16-weeks. **h,** Frequency of donor $CD45.1^+$ chimerism of bone marrow $Kit^+Sca1^+Lineage^-$ (KSL) HSPCs and peripheral blood (PB) after 16 weeks. Control n = 10 mice, *Tada2b* n = 10 mice, *Taf5l* n = 8 mice. P-value determined by paired t-test. **i,** Frequency of donor $CD45.1^+$ chimerism in the KSL, $c\text{-}Kit^+Lineage^-$ and $Lineage^+$ bone marrow populations within individual recipients after 16-weeks. Control n = 10 mice, *Tada2b* KO n = 10 mice, *Taf5l* KO n = 8 mice. P-value determined by paired t-test. **j,** Frequency of total $c\text{-}Kit^+Sca1^+Lineage^-$ HSPCs within the bone marrow of recipient mice after 16-weeks. Control n = 10 mice, *Tada2b* KO n = 10 mice, *Taf5l* KO n = 8 mice. P-value determined by ANOVA. **k-i,** White blood cell counts (**k**) and red blood cell counts (**i**) in recipient mice after 16-weeks weeks. Control n = 10 mice, *Tada2b* KO n = 10 mice, *Taf5l* KO n = 8 mice. P-value determined by ANOVA.

# Figure 3

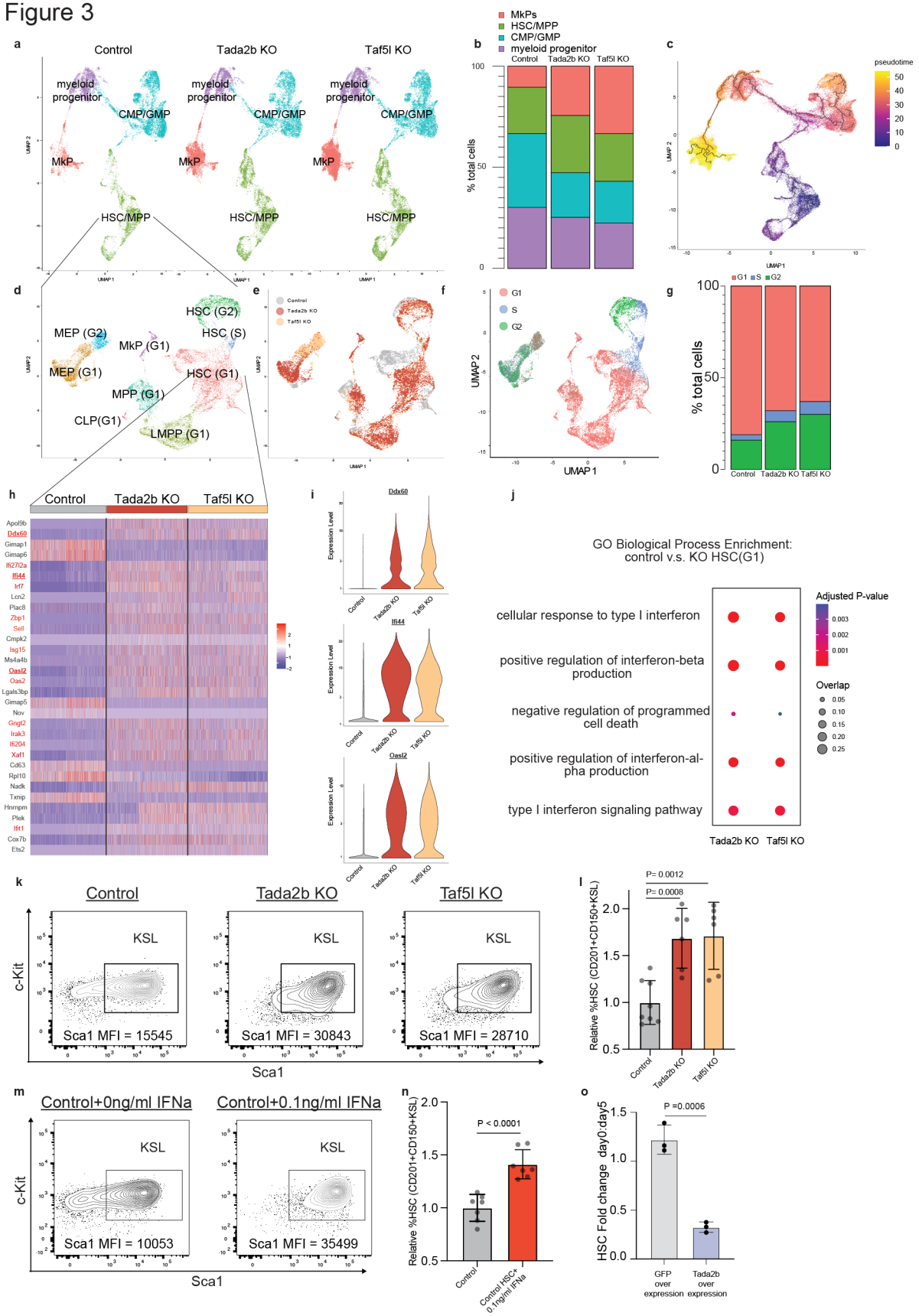

**Fig. 3: Loss of *Tada2b* and *Taf5l* enhances IFN regulated gene expression in HSCs. a,** UMAP representation of single cell RNA-seq of control, *Tada2b* KO, and *Taf5l* KO HSC cultures at day 14 with clusters annotated. Total of 61,324 single cells analyzed**. b,** Frequency of cell type clusters in the control, *Tada2b* KO, and *Taf5l* KO cultures. **c,** UMAP representations of pseudotime analysis annotated. **d-e,** UMAP representations of the HSC/MPP cluster from a following sub-clustering with cluster annotated (**d**) and cell sample origin annotated (**e**). Total of 21,344 single cell analyzed. **f**, UMAP representations from **d** with cell cycle state annotated. **g**, Frequency of G1-phase HSC, S-phase HSC, and G2-phase HSC clusters from **d** in the control, *Tada2b* KO, and *Taf5l* KO cultures. **h,** Heatmap displaying the expression of the top 30 differentially expressed genes ranked by adjusted p-value between the control, *Tada2b* KO, and *Taf5l* KO cultures within the G1-phase HSC cluster from **d**. Rows represent sub-sampled single cell gene expression values. IFN response genes highlighted are highlighted in red. **i**, Violin plots for the expression of IFN response genes *Ddx60*, *Ifi44*, and *Oasl2* in control, *Tada2b* KO and *Taf5l* KO cells within the G1-phase HSC cluster from **d**. **j**, GO enrichment analysis displaying adjusted P-value and gene-set overlap for 200 most differentially expressed genes between control and KO cells within the G1-phase HSC cluster. **k-l**, Representative flow cytometric plots (**k)** of Sca1 and c-Kit expression within the Lineage$^-$ live cells of 14-day HSC cultures, for control, *Tada2b* KO, or *Taf5l* KO cultures and quantification of CD201$^+$CD150$^+$KSL (**l**). N=6-8 per condition and p-values determined by ANOVA. **m-o**, Representative flow cytometric plots (**m**) of Sca1 and c-Kit expression within the Lineage$^-$ live cells of 14-day HSC cultures, with or without 0.1 ng/ml IFNa and quantification of CD201$^+$CD150$^+$KSL (**n**). N=7 per condition and p-values determined by paired t-test. **o,** Fold change of HSC (CD201$^+$CD150$^+$KSL) percent in ex vivo cultures with *Tada2b* or *GFP* over-expression. Three independent replicates displayed. P-values determined by paired t-test.

# Figure 4

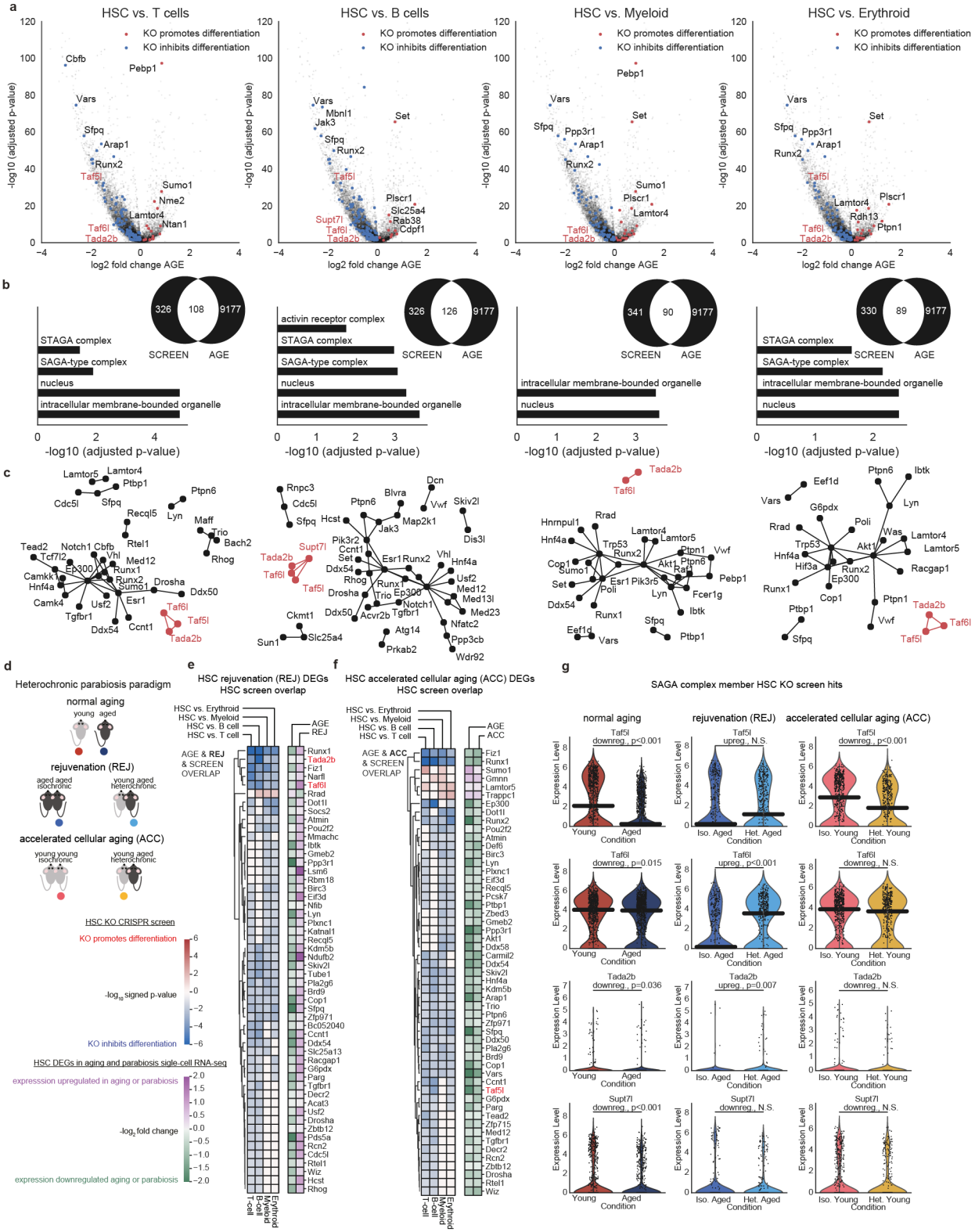

**Fig. 4. HSC KO screen hits overlap with gene expression changes in aging and heterochronic parabiosis. a**, Volcano plots indicate log2-fold changes and adjusted p-values with aging in single-cell RNAseq data[31]. 'Consistent' genes showing significant changes (adj. p-val<0.05) that have the same direction in the screen and RNAseq datasets are highlighted in red (KO promotes differentiation and the gene is upregulated with aging) and blue (KO inhibits differentiation and the gene is downregulated with aging). Top 5 up- and downregulated genes with aging are annotated. Members of the SAGA complex exhibiting consistent changes are annotated with red. **b**, Venn-diagrams show the number of screen hits, the number of differentially expressed genes in single-cell RNAseq data, and the number of 'consistent' genes between the two datasets. Bar plots indicate pathways with adj. p-value<0.05 from the Gene Ontology Cellular Components 2021 database. Pathways were determined with Enrichr based on the consistent gene sets. **c**, Force-directed network visualization of the STRING links (confidence>0.7) between the 'consistent' genes. **d**, Schematic of heterochronic parabiosis paradigm. **e,** Genes that are hits in at least two screens and consistently change in the single-cell RNAseq data with normal aging (AGE) and rejuvenation (REJ) are shown. Genes are clustered with hierarchical clustering. Leftmost four columns indicate screen related changes, while the rightmost columns indicate changes in the RNAseq data. **f**, Same as **e** for AGE and accelerated cellular aging (ACC). **g**, Violin plots for gene expression of select members the SAGA complex member in HSCs from single-cell RNAseq gene expression data[31]. Significance values show the adj. p-values of the Wilcoxon–Mann–Whitney test (two-sided) based differential gene expression.

Extended Data Figure 1

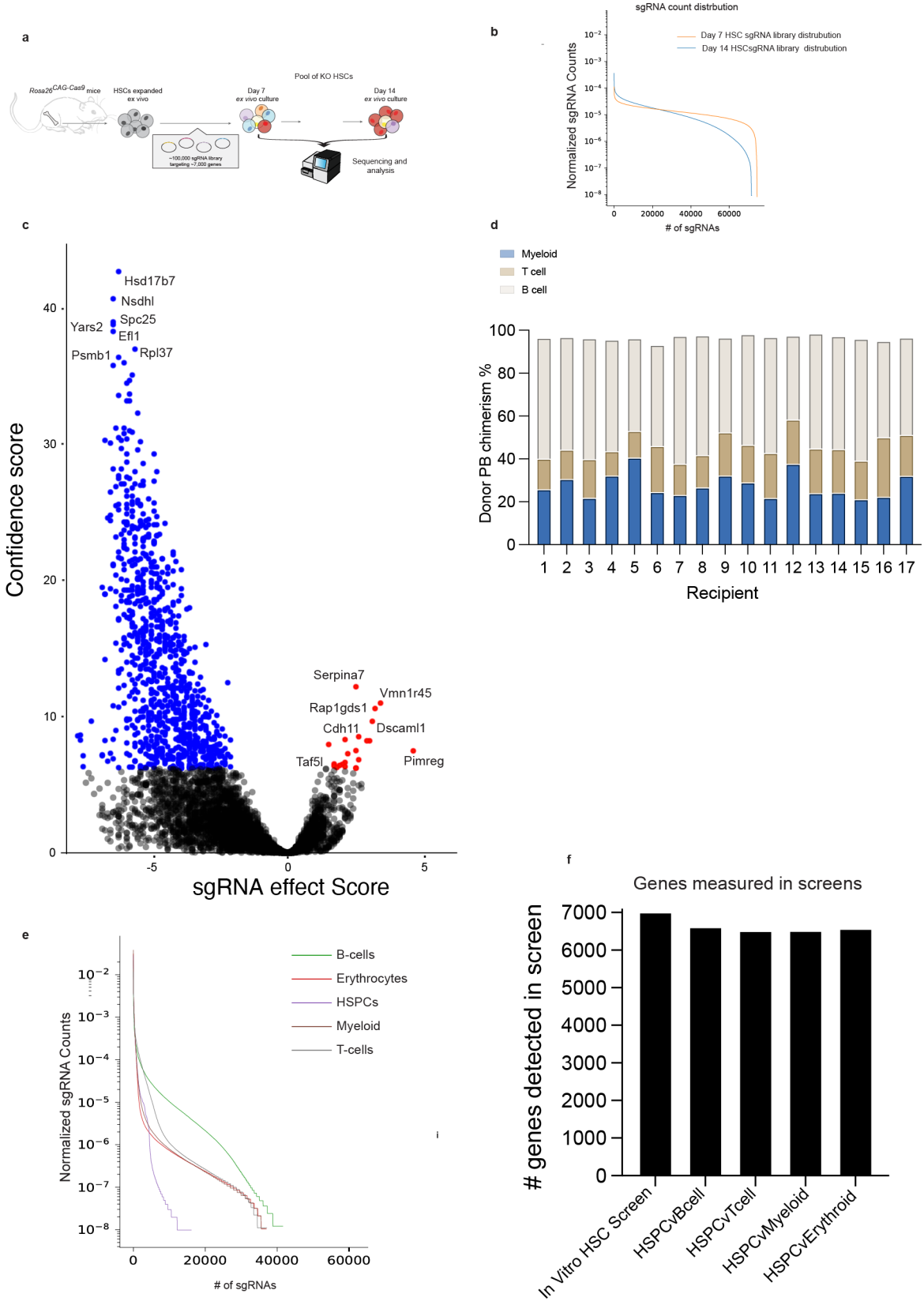

**Extended Data Fig. 1: Ex vivo HSC CRISPR KO screens reveal HSC regulators and maintain library representation. a,** Schematic of in vitro HSC CRISPR KO screens. **b,** Representation of sgRNA abundance at day 7 and day 14 post sgRNA library infection. **c**, Screen results of day 7 vs day 14 sgRNA abundance in ex vivo expansion. **d,** Flow cytometric analysis of peripheral blood chimerism of mature cell lineages of day 14 sgRNA library HSCs at 10-weeks after transplantation. **e,** Representation of sgRNA abundance of mature cell lineages at 10-weeks after transplantation. HPSC representation altered by harvesting fewer cells from bone-marrow cells. **f,** Number of genes represented in screen comparisons at 10-weeks after transplantation.

Extended Data Figure 2

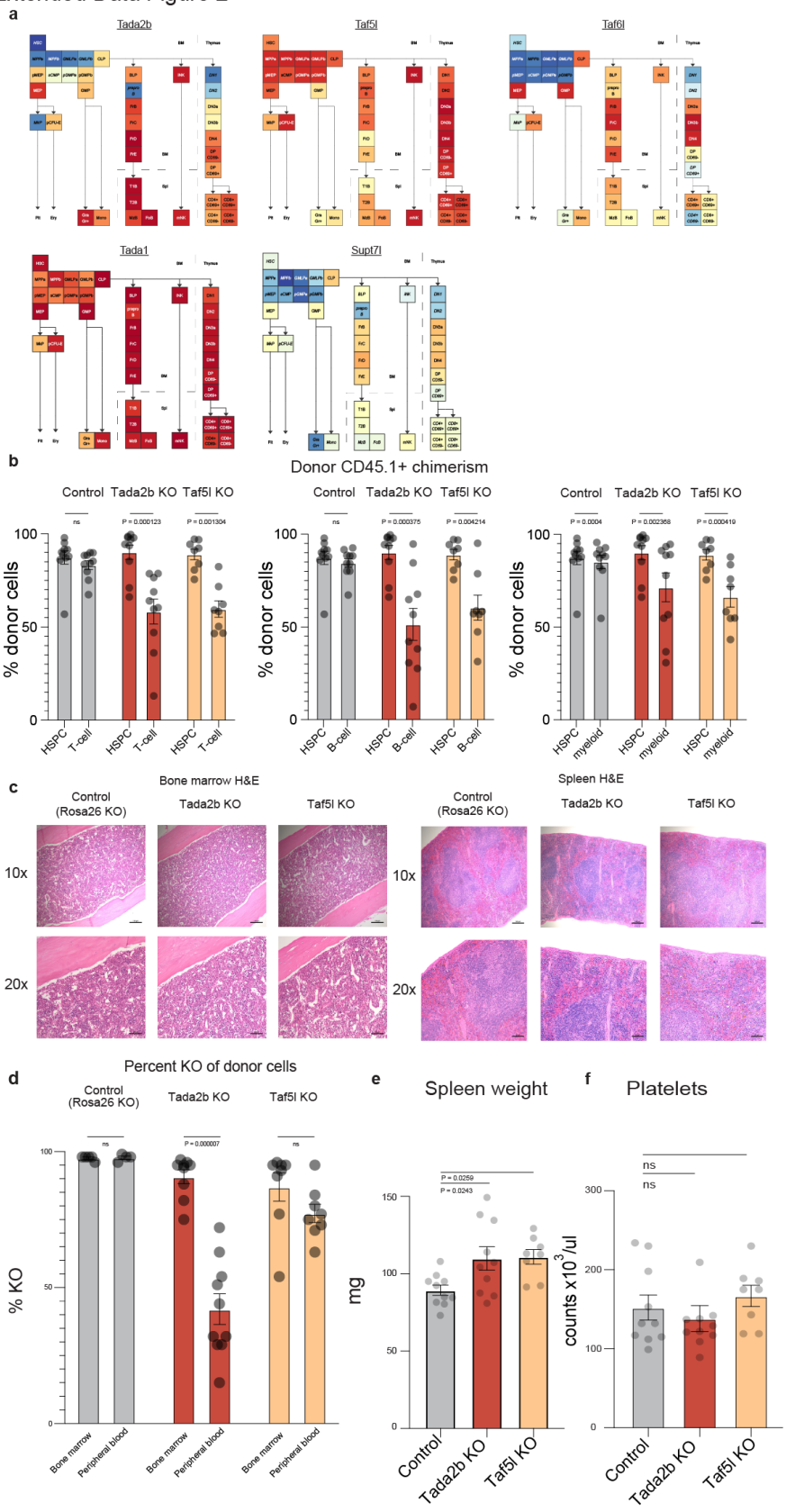

**Extended Data Fig. 2: SAGA complex members as hematopoiesis regulators. a,** Expression of SAGA complex members in hematopoiesis. Adapted from Gene expression Commons[41]. **b,** Donor cell chimerism within haematopoietic lineages in competitive KO transplant recipients. Control n = 10 mice, *Tada2b* n = 10 mice, *Taf5l* n = 8 mice. P-value determined by paired t-test. **c**, Representative H&E staining of bone marrow and spleen of *Tada2b* and *Taf5l* KO HSC recipient mice. **d,** Percentage of KO cells in Lineage$^-$c-Kit$^+$ bone marrow and peripheral blood of mice with HSC KO transplanted cells. Control n = 5 mice, *Tada2b* n = 10 mice, *Taf5l* n = 8 mice. P-value determined by paired t-test. **e,** Quantification of spleen weight in control and KO HSCs recipient mice. Control n = 10 mice, *Tada2b* n = 10 mice, *Taf5l* n = 8 mice. P-value determined by paired t-test. **f,** Quantification of platelet count in control and KO HSC recipient mice. Control n = 10 mice, *Tada2b* n = 10 mice, *Taf5l* n = 8 mice. P-value determined by paired t-test.

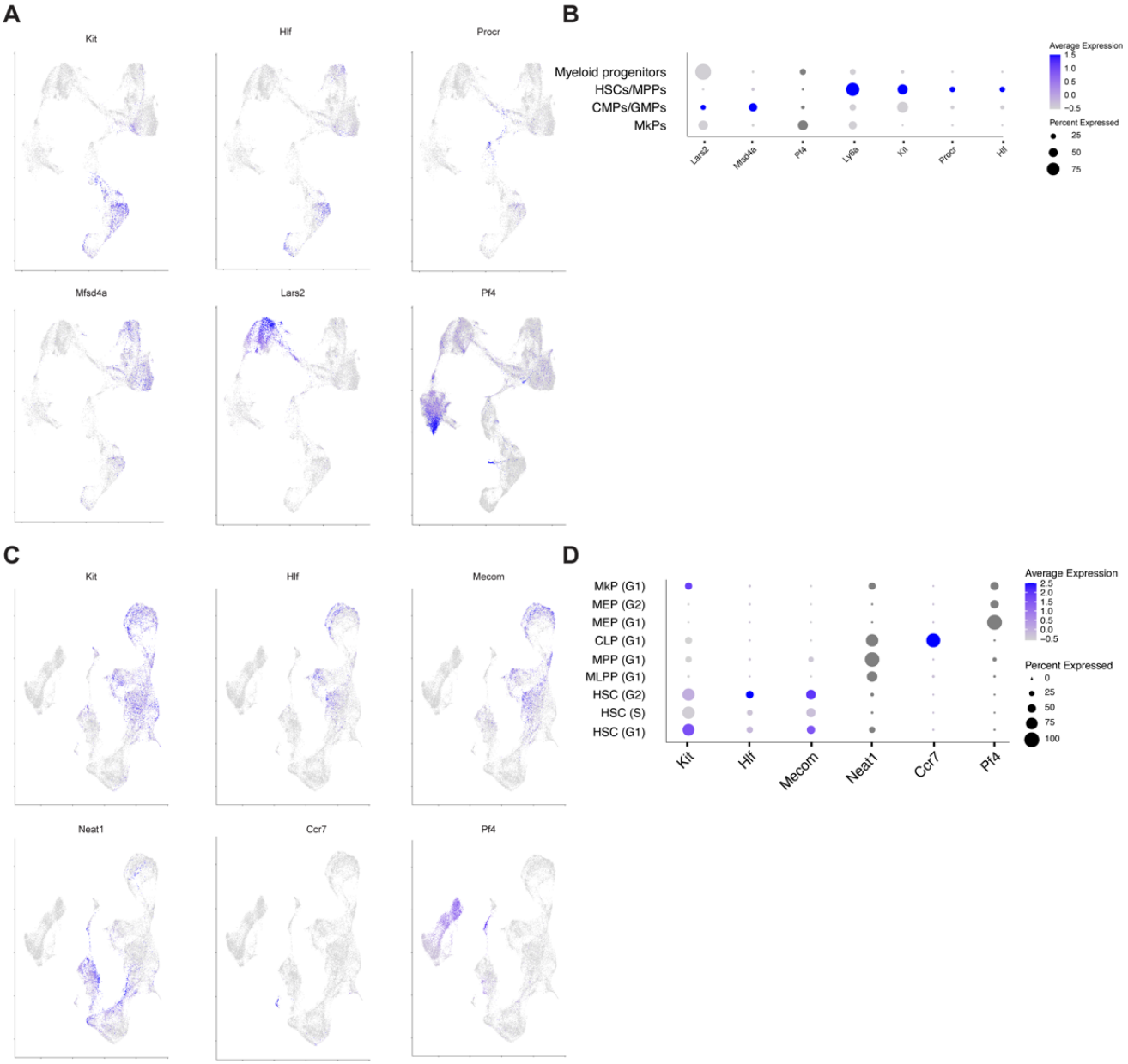


**Extended Data Fig. 3: Cell markers for single cell RNAseq clusters**
**a,** Feature plots for genes defining various clusters of all control cells with the exception of *Pf4* which contains KO cells as well. **b,** Dotplots displaying marker gene expression for various clusters of all cells. **c,** Feature plots for genes defining various clusters of all control cells within HSC subcluster. **d,** Dotplots displaying marker gene expression for various clusters of cells within HSC subcluster.

Extended Data Figure 4

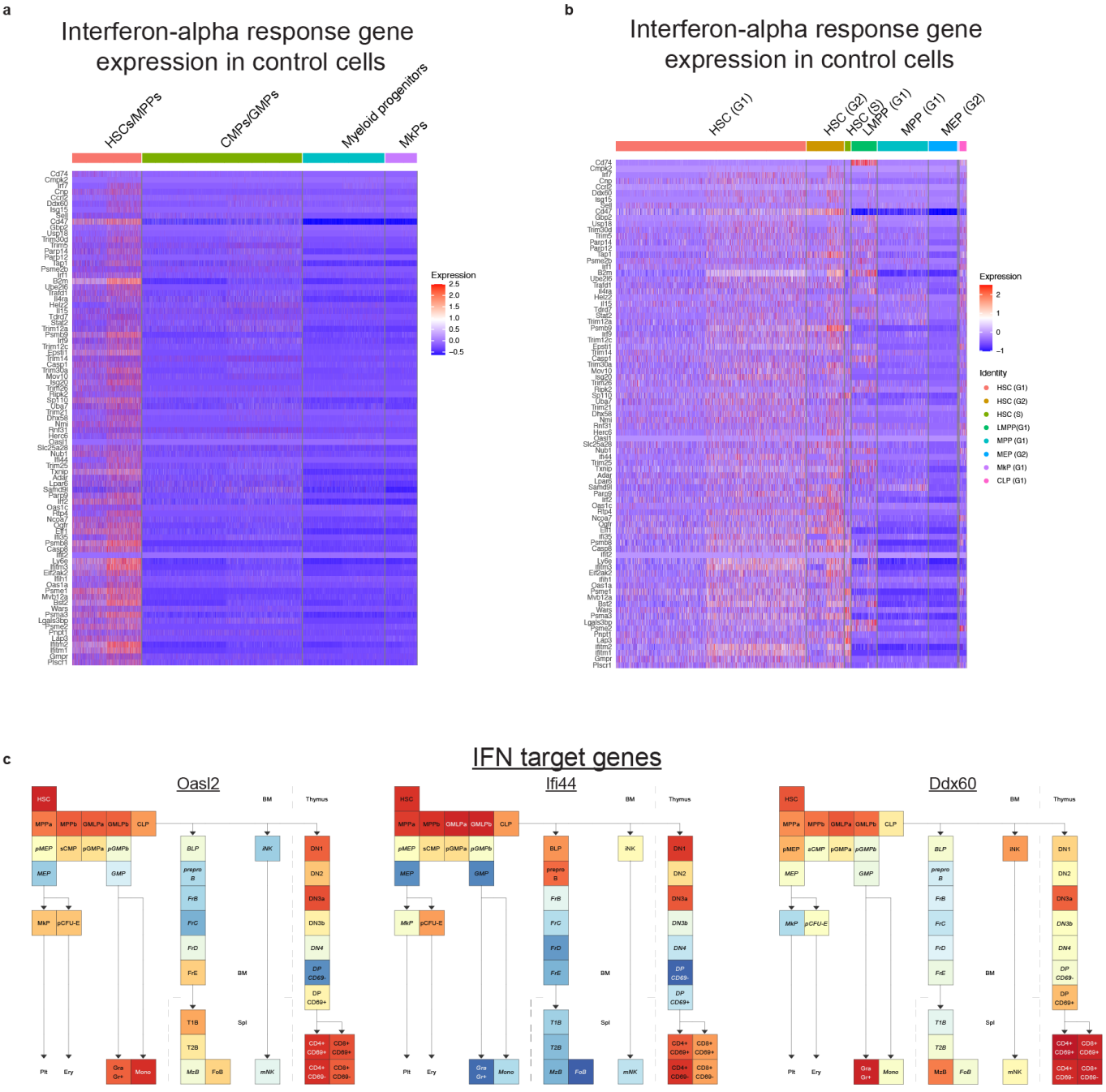


**Extended Data Fig. 4: Interferon response gene expression during hematopoiesis.** **a-b,** Heatmap displaying the expression of interferon-alpha response genes in cell clusters from **Fig. 3a** (**a**) and **Fig. 3d** (**b**) within the control sample only. **c,** Gene expression heatmap plots from adapted from Gene Expression Commons[41] displaying expression of IFN target genes *Oasl2*, *Ifi44*, and *Ddx60* in hematopoietic cell types.

**Extended Data Figure 5**

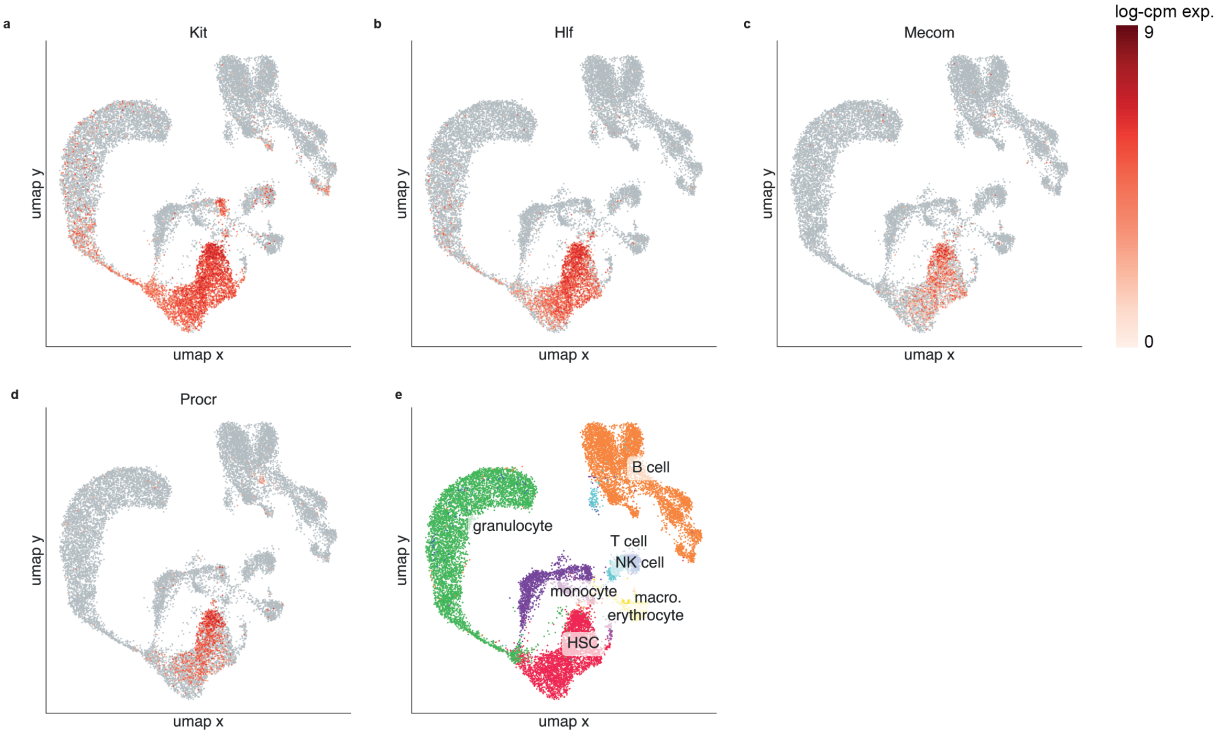


**Extended Data Fig. 5: HSC cell type identification from in vivo aging and parabiosis single-cell RNAseq datasets**

**a-d,** Feature plots of gene expression values in single cells in mouse bone marrow for the HSC marker genes *Kit* (**a**), *Hlf* (**b**), *Mecom* (**c**), and *Procr* (**d**) from a published single-cell RNAseq dataset[31]. **e,** Annotations of mouse bone marrow single cell RNA-seq data based on marker genes. Only the cluster annotated 'HSC' was used for DEG analysis in young, aged, and parabiosis mice in **Fig. 4**.